Synthesis, structure, and optical properties of nanopowders CdS: xAl (x=0, 1, 5, 10, 15 and 20%) via the sol–gel technique

E. M. Assim

Physics Department, Faculty of Education, Ain Shams University, Roxy, Cairo 11757, Egypt

The nanocrystalline Al-doped CdS semiconductors were produced accurately by the sol-gel calcination process. The aluminum was added with different percent's (0, 1, 5, 10, 15, and 20 wt%) to the synthesized CdS. Both FT-Raman analysis and UV–VIS-NIR absorption measurements were utilized to characterize the studied semiconductors' structural and optical characteristics. The detected X-ray diffraction (XRD) patterns of the prepared CdS present a polycrystalline structure, and Al-doping does not significantly impact this range. Optical bandgaps were determined for undoped and Al-doped CdS, showing a significant change with the percentage of Al-dopants. With increasing Al-doping up to (20 percent), the optical bandgap for CdS (2.38 eV) grows to reach (2.47 eV) and the allowed transitions were found to be direct for the investigated samples. The blue shift may be the reason for the optical bandgap variations. Scanning Electron Microscope (SEM) micrographs were performed to establish the Al-doped CdS nanostructure to identify the morphological characteristics.

Keywords: *Al-doped CdS; Optical properties; Spray pyrolysis; Sol-gel Technique.*

Egyptian Journal of Solids, Egypt J. Sol.

Receive Date: 30 August 2021; Revise Date: 29 September 2021; Accept Date: 30 September 2021;

Publish Date: 01 October 2021

Tel: 01002699970

Corresponding Author: Email: dr_eman_assem@hotmail.com

1.Introduction

Nanostructured semiconductors have attracted lot of interest in advanced technological applications and fundamental research because of their size-dependent uniqueness optical and electronic properties [1]. CdS is a widely utilized substance with a wide range of advanced technical applications, including solar cells, photochemical catalysis, nonlinear optical materials, gas detectors, various luminescence, and optoelectronic devices. [2-4]. It is a direct bandgap binary semiconductor and an important source for photovoltaic applications [5]. The slightly wide energy bandgap (2.42 eV) and n-type semiconducting properties make CdS a suitable alternative for several heterojunction thin-film solar cells [6]. The copper indium gallium diselenide/sulphide (CIGS), CdTe, and $CuInSe_2$ / sulphide can form the heterojunction photovoltaic cell with cadmium sulphide [7]. Doping impurity elements like indium, aluminum, gallium, and boron can promote the optical and electronic characteristics of CdS [8–11]. Also, CdSe doped with different elements for obtaining p-type CdSe or high n-type CdSe carrier concentrations such as CdSe:Sb [12], CdSe doping with Er^{3+} [13], CdSe doping with indium [14] and Ni doping [15]. Aluminum is one of these additives that can provide n-type CdS with improved electrical behavior. As free electron is generated from Al^{3+} substitution in CdS, the control in the morphology of the film, chemical composition and particle size can occur during the synthesis by adjusting the doping level. Adding cationic impurities to the CdS matrix causes the dopants substitution on cadmium sites and enhances their optoelectronic characteristics [3]. Numerous processes can be used to synthesis Al- doped CdS thin films, like spray pyrolysis, chemical bath deposition (CBD), electrodeposition, thermal evaporation, and sol-gel [16,17]. Although work on the doped CdS system has already been performed [1, 18,19], the optical, structural, and photoluminescent compatibility studies are still scarce. Consequently, in the current study, the optical, structural, and characteristics can be adapted by adding Al in different concentrations to CdS films to detect films' possible technological application feasibility.

The current research demonstrates the impact of Al doping on the structural and optical characteristics of nanocrystalline CdS. The nanopowder synthesis based on Al-doped CdS is presented through the sol-gel calcination method. X-ray diffraction XRD, FT-Raman analysis and SEM morphology of the CdS: xAl (x=0, 1, 5, 10, 15 and 20 wt %) characterized the structure. Additionally, optical constants were determined via the diffused reflectance.

2.Experimental details

2.1. Samples preparation

At the first stage, two solutions of 0.5 M of cadmium nitrate ($Cd(NO_3)_2 \cdot 4H_2O$) and 1 M of ($Na_2S \cdot 9H_2O$) were dissolved separately in deionized water using a 600 rpm/60 ^oC magnetic stirrer. The pure and Al-doped CdS were performed with the same methodology. The pure CdS was prepared by addition of 50 ml of 1 M ($Na_2S \cdot 9H_2O$) in deionized water to 100 ml of 0.5 M cadmium nitrate ($Cd(NO_3)_2 \cdot 4H_2O$) in deionized water. Cetyltrimethylammonium bromide (CTAB) has been used as a 15g / L as a surfactant. The addition takes place for one

Egyptian Journal of Solids (Egypt J Sol)

hour with continuous stirring. The final product was left again on the magnetic stirrer for another one hour with the same conditions before. When the reaction was done, the solution was naturally cooled to room temperature. After that, the final product was filtered then cleaned serval times via deionized H_2O and ethanol to get rid of unwanted residuals, followed by the drying at 100 ^oC for 48 hours.

The doping (Al $(NO_3)_3 \cdot 9H_2O$) with different concentrations (1, 5, 10, 15, and 20%) was performed with the same methodology. Addition of (Al $(NO_3)_3 \cdot 9H_2O$) as a Al^{+3} metal ions source in the molar (Al/Cd) ratio of 1%, 5%, 10%, 15% and 20% into the as-prepared solution in the same beaker. The as-prepared complexes of each molar ratio were continuously stirred for 1 h until homogenous solution was obtained.

2.2. Characterization techniques

Shimadzu Lab-X- XRD- 6000 diffractometer with a speed of 4 oC / min at 40 kV and 30 mA between 10 and 70 oC had been used for the structure characterization. Morphological and elementary characterizations were done using SEM / EDX unit JEOL JSM 6360 (Japan). Fisher selected as the sample's DXR FT-Raman spectrometer (λexc=532 nm at 5 mW power) for Raman- spectral- analysis. For the optical measurements a JASCO V- 570 UV–Vis.-NIR spectrophotometer [Japan] had been use.

3.Results and discussion

3.1.1 X-ray diffraction analysis

To explore the impact of Aluminum doping on the structure of CdS nanoparticles, the samples containing different contents of Al and the control pure CdS sample were investigated via X-ray diffraction. As shown in Fig. 1, all samples have four perspicuous diffraction peaks, indicating their polycrystalline character and the films behavior with Al doping does not change which agrees with previously published data from Bairy et al., [20]. The XRD patterns to all investigated samples agree well with the hexagonal CdS structure of diffractogram (JCPDS 41-1049), and exhibit diffraction peaks at angles ($2\theta^{\circ}$) of 27.26, 44.70, 47.60, and 52.30, which can be indexed as (002), (110), (103) and (201) planes, respectively [21]. No characteristic peak was observed for other impurities in the all samples, demonstrating the purity of the samples prepared by sol-gel calcination method. It is also obvious that the addition of Al up to 20 wt % to CdS NPs cannot change the uniform single-phase hexagonal CdS crystals [22].

Using the most intensive diffraction peak of CdS at (2θ =27.26◦), the values of the interplanar distance (d) for pure and Al-doped CdS samples are listed in Table (1). The intensity of Al doped samples along (002) plane is increased with increasing Al content which can be attributed to the replacement of Cd^{+2} ions by Al^{+3} ions in the CdS lattice.

The interplanar distance (d) in CdS is slightly changed after doping with Al because the ionic radii of the elements Al^{+3}(0.53 Å) and Cd^{+2}(0.95 Å) have a significant difference, which means that aluminum ions can enter interstitially and substitutionally in the crystalline structure of CdS [23]. Also, the average crystallite size *D* estimated from Scherrer's relation:

Egyptian Journal of Solids (Egypt.J.Sol)

$$D = \frac{0.9\,\lambda}{\beta \cos\theta} \qquad (1)$$

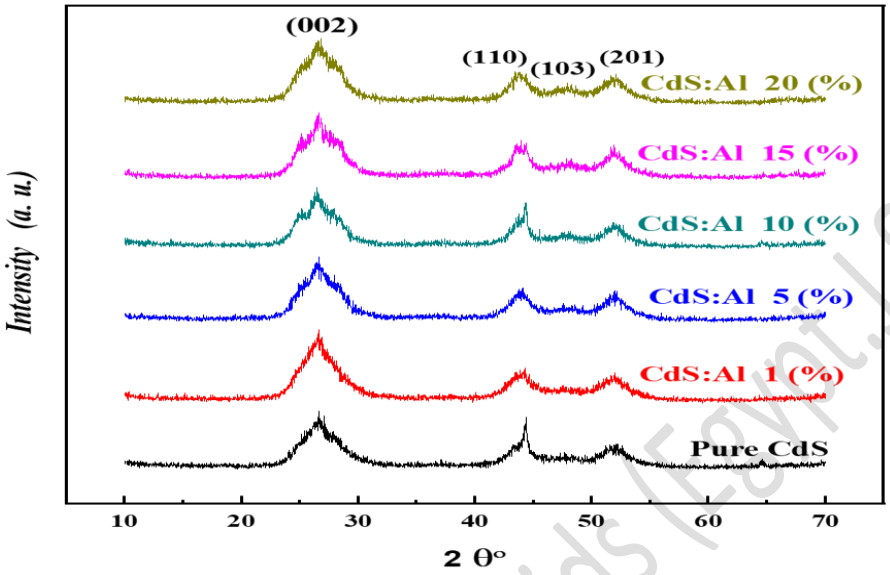

Fig. 1. The X-ray diffraction patterns for *CdS: xAl (x=0, 1, 5, 10, 15 and 20 wt %)* nanostructure.

where, β is the full width at half maximum (FWHM) of the diffraction peak in radian and λ =0.15418 nm is the X-ray wavelength. The obtained values of *D* are compared with the results of pure CdS hexagonal nanocrystals prepared by several methods in previous articles (~ 3 – 47 nm) [24-26]. The average crystallite size *D* for pure and Al-doped CdS is almost unchanged (~ 34 nm) which supported that the crystals are in hexagonal structure.

Table 1: The values of the interplanar distance (d) and the average crystallite size D for pure and Al-doped CdS samples.

Samples	X- ray diffraction angle $2\theta^{\circ}$	Interplanar distance d (nm)	Average crystallite size *D* (nm)
Pure CdS	27.26	0.3273	34.2
1 wt% CdS:Al	27.35	0.3262	34.1
5 wt% CdS:Al	27.37	0.3259	34.3
10 wt% CdS:Al	27.33	0.3260	34.3
15wt% CdS:Al	27.36	0.3258	34.4
20wt% CdS:Al	27.38	0.3255	34.4

Egyptian Journal of Solids (Egypt. J. Sol)

3.1.2 Morphological characteristics

Fig. 2 (a,b,c,d,and e) illustrates SEM images of Al-doped CdS (0, 1, 5, 10, and 20 wt%) nanopowders synthesized via the sol-gel calcination method respectively. The particles, in all cases, microscopically agglomerate to create a single, smooth film. Though the films display the grain size decrease initially, it stabilizes as the Al doping percentage increases, and therefore the particle density increases. The films' average grain size is within 50 nm for all the samples while agglomerated, and the nanoclusters' size can be between 100 and 300 nm. Sonker et al. [27] reached the close particle diameter (40-60 nm) for CdS nanoparticles produced by utilizing the chemical route technique. In a recent study, a similar morphology for doped CdS films was reported [28].

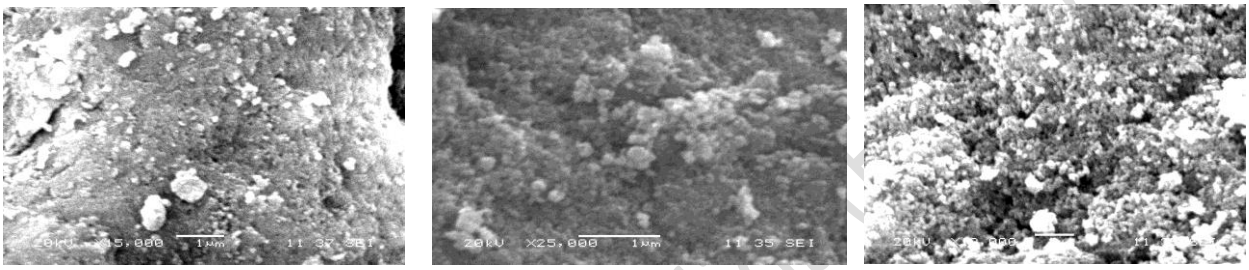

(a)pure CdS **(b)1 wt% CdS: Al** **(c) 5 wt% CdS: Al**

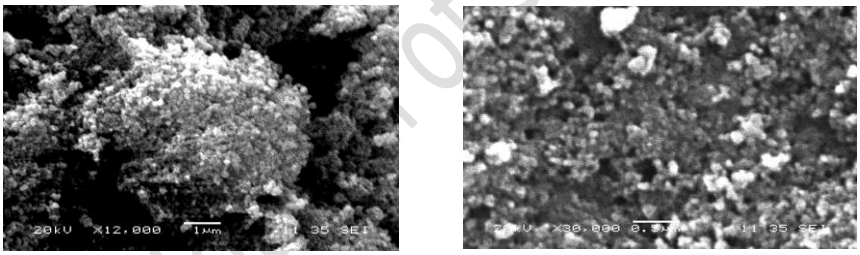

(d) 10 wt% CdS: Al **(e) 20 wt% CdS: Al**

Fig. 2. The SEM for undoped CdS and Al-doped CdS nanostructure.

3.1.3 Vibrational analysis

Raman spectroscopy is usually helpful in determining dopants, crystal lattice defects, and orientation. The FT-Raman vibrational spectra exhibited in Fig. 3 for Al- doped CdS (0, 1, 5, 10, 15, and 20 wt %) nanopowders synthesized by the sol-gel calcination method, within 100–1000 cm^{-1} range. Two distinct Raman peaks declare at approximately 300 and 598 cm^{-1}. The high-intensity peak at 300 ± 3 cm^{-1} presents the longitudinal optical phonon mode (1LO). For the higher aluminum concentration (20 %), this band exists at 310 cm^{-1}. The low-intensity band appears at 598 ± 4 cm^{-1} (2LO). Muthusamy et al. and other researchers have reported a similar peak position [29,30]. About 7 cm^{-1} shift in the Raman spectra of pure

CdS compared to a shift of 20 wt% Al-containing sample because of the particle size effect. As the nano-sized grains significantly influence vibrational properties, the nanoscale of the particles creates asymmetry and a Raman shift near the lower frequency, as Richter et al. have demonstrated. [31].

Table (2) indicates the analysis of Raman spectra for the investigated samples as the doping concentration varies. The sample containing 20 wt% Al with the maximum particle size recorded the higher band values for both (1LO) and (2LO) longitudinal optical phonon modes. The other samples have a small shift in their positions. This means that the produced samples are almost impurities-free, and the dopant impact on the matrix causes the small shift, which leads to relatively slight strain distortions. The polarizing field of LO phonon on the surface of particles coupled electron and hole pairs, resulting in a large value of electron–phonon interaction strength.

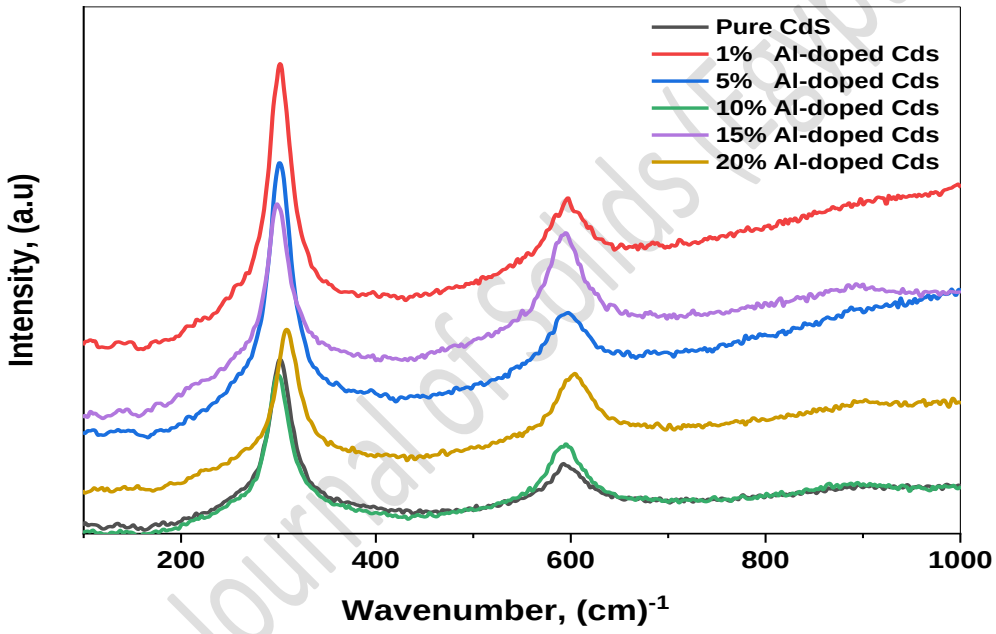

Fig. 3. FT-Raman shift of CdS: xAl (x=0, 1, 5, 10, 15 and 20 wt %) nanostructure.

Egyptian Journal of Solids (Egypt.J.Sol)

Table 2: Raman spectroscopy analysis of pure and Al-doped CdS samples.

Samples	1LO peaks position (cm) $^{-1}$	2LO peaks position (cm) $^{-1}$
Pure CdS	303	594
1 wt% CdS:Al	302	597
5 wt% CdS:Al	300	596
10 wt% CdS:Al	300	594
15wt% CdS:Al	297	594
20wt% CdS:Al	310	602

3.2 Optical properties of undoped and Al-doped CdS nanopowders

In different spectral ranges, Diffuse reflectance (DR) consider an effective method for crystalline nanostructured substances in powdered form. The incident radiation in external reflection concentrates on the sample, and two reflection forms, i.e., diffuse, and specular, can occur. The light component reflected in all paths during the penetration of the incident beam energy to a particle or several particles is Known as diffuse reflectance. Many specimens can generate diffuse spectra such as powders, fibers, or rough surface materials like textiles [32]. Diffuse reflection is only the beam portion, which is dispersed and brought back to the sample surface. Many powders may be examined as tidy samples by diffuse reflection (soil samples, coal samples, transparent diffuse coatings). The reflections are specular, a non-destructive surface measurement method utilizing a mirror like reflection from a matte surface or sample's shiny [32,33]. The Kubelka – Munk theory examines diffuse reflectance spectra obtained from weakly absorbing samples in general. At any wavelength, Kubelka – Munk equation can be in the form [33,34]:

$$F(R) = \frac{(1-R)^2}{2R} \qquad (2)$$

F(R) symbolize to the Kubelka–Munk function, and R symbolize to the absolute reflectance of the specimen. The diffused reflectance plots for undoped and Al-doped CdS nanopowders are obvious in Fig. 4. It is clear from this Fig., that the diffused reflectance increases as wavelengths grow. Incorporating Al dopants into the host CdS often increases diffused reflectance for Al-doped CdS with 1–20 percent concentrations. As obvious in Fig. 4, as the concentration of Al dopants increases, the edge of absorption shifts sharply.

The *F(R)* values were transformed to the linear absorption coefficient as follow [34]:

$$\alpha = \frac{F(R)}{t} = \frac{absorbance}{t} \qquad (3)$$

where *t* is the pellet thickness, it is in the range of 0.5 mm.

Egyptian Journal of Solids (Egypt. J. Sol.)

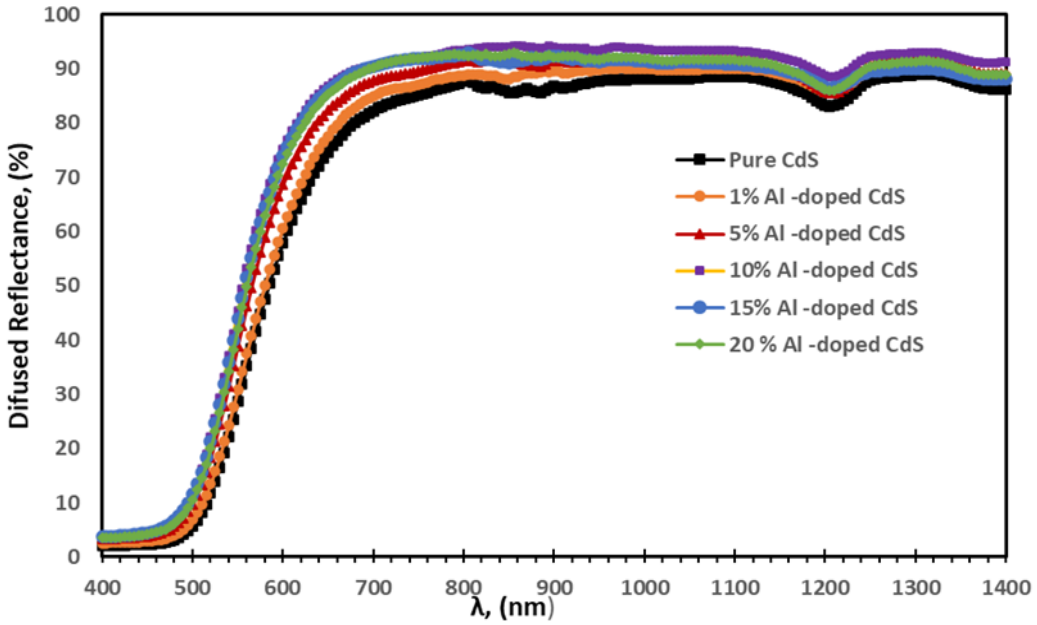

Fig. 4. ***Reflectance plots of CdS: xAl (x=0, 1, 5, 10, 15 and 20 wt %) nanostructure.***

Based on the diffused reflectance data, the next equation can be used to estimate the value of the index of absorption k:

$$\mathbf{k}=\frac{\boldsymbol{\alpha\lambda}}{\boldsymbol{4\pi}} \quad (4)$$

The absorption index k versus wavelength is graphically represented in Figure 5. Compared with Al-doped CdS nanopowders, undoped CdS nanopowders' absorption index is very high. Such lower absorption index values are compatible with the optical constants' measurements dependent on the diffused reflectance. As evidence, for the diffuse reflectance evaluation of the weak absorbing materials, the Kubelka – Munk theory can be employed.

Both direct and indirect optical transitions occur in semiconductor materials. Corresponding to the electron's excitation inside the band gap from valance to conduction band, the optical bandgap E_g can be estimated using the fundamental absorption. The optical bandgap can then be calculated using the form below [35]:

$$(\alpha h\upsilon) = A(h\upsilon - E_g)^n \quad (5)$$

For the diffused reflectance measurements, the previous Eq. can be introduced in the form [36]:

$$(\alpha h\upsilon) = \frac{F(R)h\upsilon}{t} = A(h\upsilon - E_g)^n \quad (6)$$

Egyptian Journal of Solids

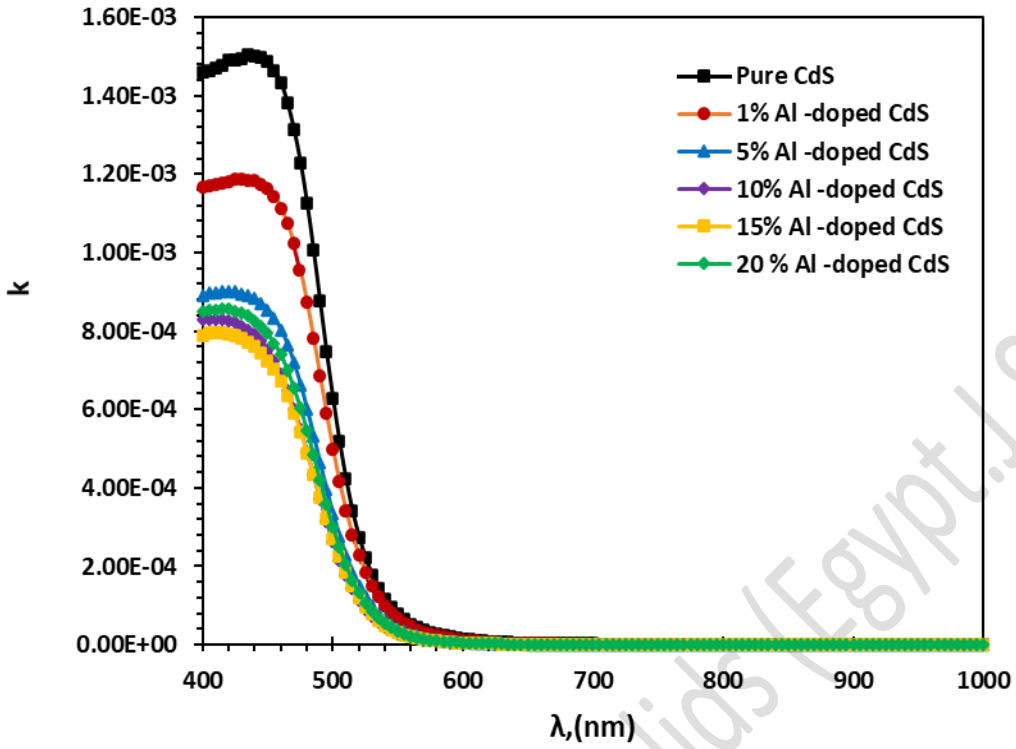

Fig. 5. Absorption index(k) of CdS: xAl (x=0, 1, 5, 10, 15 and 20 wt %) nanostructure.

where E_g is the optical bandgap, *hu* symbolizes the incident photon energy, α symbolize the absorption coefficient, while *A* is a constant that reliant on the transition probability. The parameter *n* characterizes the optical absorption process and reliant on the type of electronic transition that causes absorption. It has values 2 for indirect transition and 1/2 for the direct transition, at which the absorption is due to differences in both conduction and valence bands between extended states. The typical way to estimate the optical bandgap value is to plot $(\alpha h\upsilon)^{1/2}$ against $(h\upsilon)$. The relations $(\alpha h\upsilon)^{1/2}$ and $(F(R)h\upsilon/t)^2$ versus $(h\upsilon)$ are illustrated in Figures (6) and (7), respectively. Fig. (7) indicates that the relation $((F(R)h\upsilon/t)^2$ versus $(h\upsilon)$ is linear, which proves that the allowed transitions are direct for the investigated samples. From the plots of $(F(R)\ h\upsilon/t)^2$ as a function of photon energy $h\upsilon$ (Fig. 7), the optical bandgap of the samples was calculated. The optical bandgap values for pure and Al- doped CdS were obtained from the linear portion's extrapolation of these plots to the x-axis, as clear in Table (3). In detail, the optical bandgap of the undoped CdS sample is 2.38 eV. Also, the optical bandgap E_g rises from (2.38 eV) to (2.47 eV) by 20 percent of the doped sample as shown in Fig.8, which is in line with the bandgap described above [37]. That is much the same as the value previously revealed for CdS thin film [38], CdS:Sm 2.4 eV [39], Significantly more than CdS:Gd 2.3 eV [40] and bulk CdS 2.42 eV [41].

Egyptian Journal of Solids (Egypt.J.Sol)

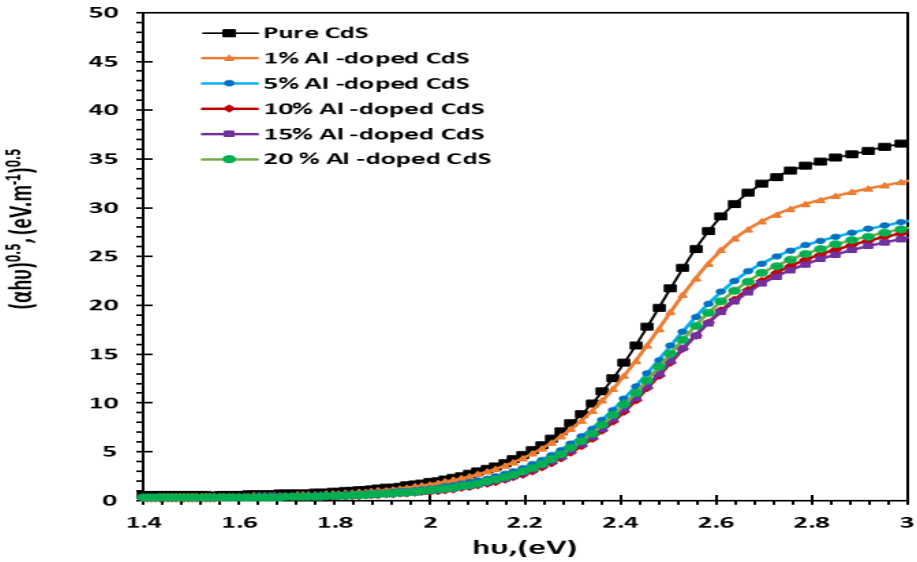

Fig. 6. The Plot of $(\alpha h\nu)^{0.5}$ versus the photon energy(hν) forCdS: xAl (x=0, 1, 5, 10, 15 and 20 wt %) nanostructure

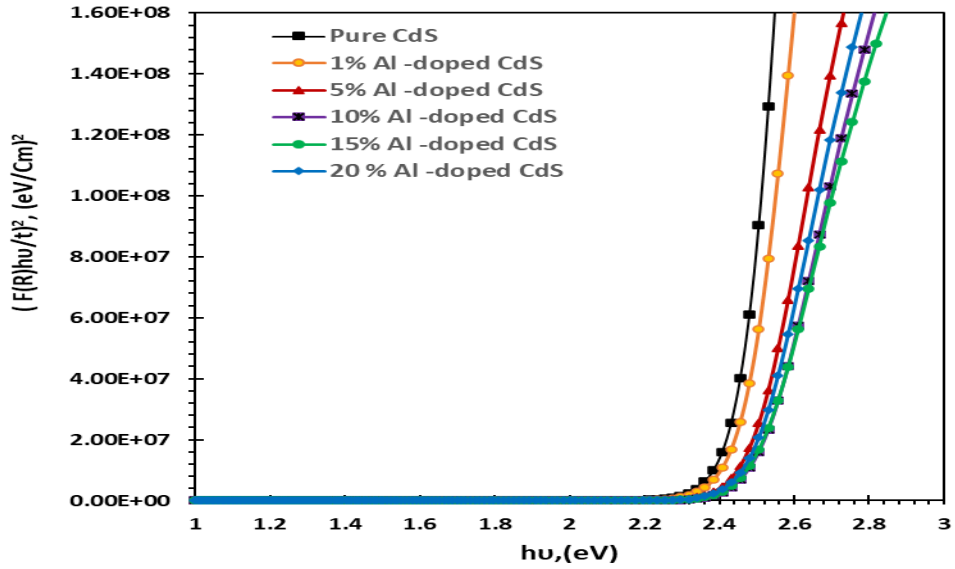

Fig. 7. The Plot of $(F(R)h\nu)^2$ /t^2 versus the photon energy for CdS: xAl (x=0, 1, 5, 10, 15 and 20 wt %) nanostructure

Table 3: The values of activation energy E_g for pure and Al-doped CdS samples.

Doped %	Pure CdS	1wt% CdS:Al	5wt% CdS:Al	10wt% CdS:Al	15wt% CdS:Al	20wt% CdS:Al
E_g (eV)	2.38	2.40	2.43	2.45	2.47	2.47

The Al-doped CdS band gap energy increases by about 0.09 eV by the increased of Al content to 20% which confirming the blue shift observed on the absorption edge spectra absorption. Similarly, the increase in optical bandgaps with increasing Cr-doped ZnO is attributed to quantum confinement of carriers ascribed to particle size effect and structural defects, according to the results [42]. Many researchers observed the same behavior by doping In, Mg, Al and Fe to ZnO and TiO_2 nanopowders respectively [43-46] . Burstein – Moss effect is found to be an explanation for the blue shift of the Al-doped CdS nanopowders optical absorption edge [47,48]. From the values of the Pauling ionic radius (in Å): Al^{3+} ($r^+ = 0.53$), Cd^{2+} ($r^+ = 0.95$) and S^{2-} ($r^- = 1.84$).

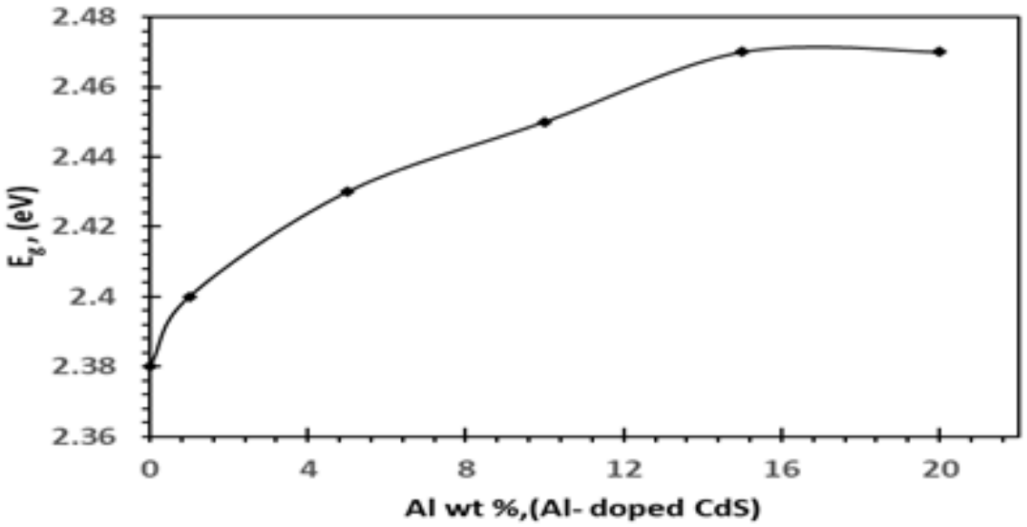

Fig. 8 .The Activation Energy as a function of Al % for undoped and Al- doped CdS nanostructure

By finding for each structure that the ratio (r^+/r^-) for which the anions just touch one another while contacting the cation, with perfect packing. The ratio (r^+/r^-) for Al-S is 3.680 and for Cd-S is 1.927. In Al_2S_3 aluminum sulphide, the small size of Al relative to sulphur dictates tetrahedral coordination, while CdS behaves as hexagonal structure [49]. Another factor the Aluminum Al^{3+} has Lewis's acid property rather than cadmium Cd^{2+} [50]. The structure of the CdS:Al is slight changes with increasing the concentration of Al^{3+}. This

gradual shift is observed in the Raman spectra (Fig.(3)&Table(2)), Which is consistent with the slight change in the values of the CdS:Al optical band gap E_g.

4. Conclusion

The sol-gel calcination technique was used to produce Al-doped CdS semiconducting nanopowders experimentally. Various spectroscopic measurements have been used to support the nanopowder structure of undoped and Al-doped CdS nanopowders. Besides, FT-Raman analysis of CdS-specimens with Al-doping show spherical grains of different sizes. A graduation shift was observed in the Rman spectra indicating a slight change structure of the CdS:Al with increasing the concentration of Al^{3+} . The undoped and Al-doped CdS nanopowders' surface morphology was studied. Optical bandgaps were determined for undoped and Al-doped CdS, showing a slightly change with the percentage of Al-dopants, which is consistent with the week change that occurred with the structural properties. The semiconductor-metal transition caused by increased doping concentration is responsible for the change in the optical absorption edge to the blue shift. This blue shift is also caused by the rise in free electrons due to Al-doping according to the Burstein – Moss effect.

Acknowledgments

The author is thankful to the ***NLEBA*** - Nanoscience Laboratory for Environmental & Biomedical Applications Nanoscience, Semiconductor Lab., Ain Shams University, Faculty of Education, Department of Physics, in addition to ***AFMOL***- Advanced Functional Materials & Optoelectronic Laboratory, King Khalid University, Faculty of Science, Department of Physics for the valuable assistance in this research paper.

References

[1] A. Khare, Factors affecting the electro-optical and structural characteristics of nano crystalline Cu doped (Cd–Zn) S films, J. Phys. Chem. Solids, 73 (2012) 839–845.

[2] M. A. Manthrammel, V. Ganesh, S. Mohd, I. S. Yahia, S. AlFalfy, Facile synthesis of La-doped CdS nanoparticles by microwave assisted co-precipitation technique for optoelectronic application, Mater. Res. Express, 6(2018)025022-025029.

[3] J.S. Jie, W.J. Zhang, Y. Jiang, X.M. Merag, Y.Q. Li, S.T. Lee, Photoconductive characteristics of single-crystal CdS nanoribbons, Nano Lett., 6 (2006) 1887–1892.

[4] M. Muthusamy, S. Muthukumaran, M. Ashokkumar, Composition dependent optical, structural and photoluminescence behaviour of CdS:Al thin films by chemical bath deposition method. Ceramics International, 40 (2014) 10657–10666.

[5] G. Perna, V. Capozzi, M. Ambrico, V. Ligonze, A. Minafra, L.Schiavulli, M. Pallara, Structural and optical characterization of undoped and indium-doped CdS films grown by pulsed laser deposition, Thin Solid Films, 453 (2004) 187-194.

Egyptian Journal of Solids (Egypt. J. Sol.)

[6] H. Chavez, M. Jordan, J.C. McClure, G. Lush, V.P. Singh, Physical and electrical characterization of CdS films deposited by vacuum evaporation, solution growth and spray pyrolysis, J. Mater. Sci. Mater. Electron., 8 (1997) 151–154.

[7] F.Lisco, P.M.Kaminski, A.Abbas, K.Bass, J.W.Bowers, G.Claudio, M.Losurdo, J.M.Walls, The structural properties of CdS deposited by chemical bath deposition and pulsed direct current magnetron sputtering , Thin Solid Films, 582(2015)323-327.

[8] K.K. Challa, E. Magnone, E.-T. Kim, Highly photosensitive properties of CdS thin flms doped with boron in high doping levels. Mater. Lett., 85 (2012) 135-137.

[9] P.K. Singh, P. Kumar, T. Seth, H.-W. Rhee, B. Bhattacharya, Preparation, characterization, and application of Nano CdS doped with alum composite electrolyte. J. Phys. Chem. Solids, 73(2012) 1159-1163.

[10] S. Butt, N.A. Shah, A. Nazir, Z. Ali, A. Maqsood, Influence of film thickness and In-doping on physical properties of CdS thin films. J. Alloy. Compd., 587(2014) 582-587.

[11] A. Fernández-Pérez, C. Navarrete, P. Valenzuela, W. Gacitúa, E. Mosquera, H. Fernández, Characterization of chemically deposited aluminum-doped CdS thin films with post-deposition thermal annealing. Thin Solid Films, 623(2017)127-134.

[12] E. U. Masumdar, V. B. Gaikwad, V. B. Pujari, P. D. More, L. P. Deshmukh, Some studies on chemically synthesized antimony-doped CdSe thin films, J. Materials Chemistry and Physics, 77(2003)669-676.

[13] R.B. López-Flores, Oscar Portillo Moreno, R. Lozada-Morales, R. Palomino-Merino, The effect of Er3+ doping on the physical properties of CdSe thin films deposited by chemical bath, Revista Mexicana de Fisica, 52 (2006) 39-41.

[14] A. M. Perez Gonzalez, I.V. Arreola, C.S. Tepantlán, Effects of indium doping on the structural and optical properties of CdSe thin films deposited by chemical bath, Revi. Mexican defisica.,55 (2009)51-54.

[15] R.R.Pawar, R. A. Bhavsar, S.G. Sonawane, Structural and optical properties of chemical bath deposited Ni doped Cd–Se thin films, Indian J.Phys.,86(2012)871-876.

[16] G. Ojeda-Barrero, A.I. Oliva-Avilés, A.I. Oliva, R.D. Maldonado, M. Acosta, G.M. Alonzo-Medina, Efect of the substrate temperature on the physical properties of sprayed-CdS flms by using an automatized perfume atomizer. Mater. Sci. Semicond. Process., 79 (2018)7-13.

[17] S. K. Panda, S. Chakrabarti, A. Ganguly, and S. Chaudhuri, Photoluminescence and Raman Study of CdS–Al2O3 Nanocomposite Films Prepared by Sol-Gel Techniques. Journal of Nanoscience and Nanotechnology, 5 (2005) 459–465.

[18] Ziaul Raza Khan, Munirah, Anver Aziz, Mohd. Shahid Khan, Sol-gel derived CdS nanocrystalline thin films: optical and photoconduction properties. Materials Science-Poland, 36 (2018) 235-241.

[19] M. Aslam Manthrammel, Mohd. Shkir, S. Shafik, Mohd. Anis, S. AlFaify, A systematic investigation on physical properties of spray pyrolysis–fabricated CdS thin films for opto-nonlinear applications: An effect of Na doping. Journal of materials research, 35 (2020) 410-421.

[20] Raghavendra Bairy, A. Jayarama, G.K. Shivakumrr, D. Suresh Kulkarni, R. Shivaraj Maidur, Parutagouda Shankaragouda Patil, Physica B: Condensed Matter, 555(2019)145-151.

Egyptian Journal of Solids (Egypt J. Sol)

[21] Lakshmi Kumari, Asit Kumar Kar, Role of PVA capping on photophysical properties of chemically prepared CdS nanomaterials: Insights on energy transfer mechanisms in the capped system, Materials Letters, 302(2021)130398.

[22] M. Muthusamy, S. Muthukumaran, Effect of Cu-doping on structural, optical and photoluminescence properties of CdS thin films. Opt. Int. J. Light Electron. Opt., 126 (2015) 5200–5206.

[23] F.J. Willars-Rodríguez , I.R. Ch_avez-Urbiola , R. Ramírez-Bon , P.Vorobiev , Yu.V. Vorobiev, Effects of aluminum doping in CdS thin films prepared by CBD and the performance on Schottky diodes TCO/CdS:Al/C, Journal of Alloys and Compounds 817 (2020) 152740.

[24] Kadir Erturk, Seref Isik, Omur Aras, Yunus Kaya, Investigation of structural, spectral, optical and nonlinear optical properties of nanocrystal CdS: Electrodeposition and quantum mechanical studies, Optik, 243(2021)167469.
[25] K. Venkatapathy, C.J. Magesh, G. Lavanya, P.T. Perumal, R. Sathishkumar, A nanocrystalline CdS thin film as a heterogeneous, recyclable catalyst for effective synthesis of dihydropyrimidinones and a new class of carbazolyl dihydropyrimidinones via an improved Biginelli protocol, N. J. Chem., 43 (2019) 10989–11002.
[26] H.S.H. Mohamed, M. Rabia, M. Shaban, S. Taha, Controlled synthesis of CdS nanoflowers thin films for H2 electro-generation, Mater. Sci. Semicond. Process., 120 (2020), 105307.

[27] Rakesh K. Sonker, B.C. Yadav, Vinay Gupta, Monika Tomar, Synthesis of CdS nanoparticle by sol-gel method as low temperature NO2 sensor, Materials Chemistry and Physics, 239 (2020)121975

[28] Mohd Shkir, Kamlesh V. Chandekar, Aslam Khan, Ahmed Mohamed El-Toni, I.M. Ashraf, M. Benghanem, Syed Farooq Adil, Anees A. Ansari, Hamid Ghaithan, S. AlFaify, Structural, morphological, vibrational, optical, and nonlinear characteristics of spray pyrolyzed CdS thin films: Effect of Gd doping content. Materials Chemistry and Physics, 255 (2020) 123615.

[29] M. Muthusamy, S. Muthukumaran, Effect of Cu-doping on structural, optical and photoluminescence properties of CdS thin films, Optik, 126 (2015)5200–5206.

[30] V.M. Dzhagan, M.Y. Valakh, C. Himcinschi, A.G. Milekhin, D. Solonenko, N. A. Yeryukov, O.E. Raevskaya, O.L. Stroyuk, D.R.T. Zahn, J. Phys. Chem. C, 118(2014) 19492–19497

[31] Richter H, Wang ZP, Ley L: The one phonon Raman spectrum in microcrystalline silicon, Solid State Communications, 39(1981) 625–629.

[32] J. Dahm Donald, D. Dahm Kevin, Interpreting Diffuse Reflectance and Transmittance: a Theoretical Introduction to Absorption Spectroscopy of Scattering Materials, Chichester, UK: NIR Publications; 2007.

[33] P.Kubelka, F. Munk , Ein Beitrag Zur Optik Der Farbanstriche. Zeitschrift für Technische Physik,12(1931) 593-601.

[34] F. Yakuphanoglu, Electrical characterization and device characterization of ZnO microring shaped films by sol–gel method Journal of Alloys and Compounds,507(2010) 184-189.

[35] F. Urbach, The Long-Wavelength Edge of Photographic Sensitivity and of the Electronic Absorption of Solids, Physical Review, 92(1953)1324.

[36] R. Köferstein, L. Jäger, SG. Ebbinghaus, Magnetic and optical investigations on $LaFeO_3$ powders with different particle sizes and corresponding ceramics, Solid State Ionics, 249–250(2013)1–5.

Egyptian Journal of Solids (Egypt J Sol)

[37] M.Aslam Manthrammel, Mohd. Shkir, Mohd Anis, S.S.Shaikh, H.Elhosiny Ali, S. Alfaify, Facile spray pyrolysis fabrication of Al_CdS thin films and their key linear and third order nonlinear optical analysis for optoelectronic applications, Optical Materials, 100(2020)109696.

[38] A.I. OlivaSolıXO, R. s-Canto, X.R. Castro, P. Guez Quintana, Formation of the band gap energy on CdS thin films growth by two different techniques. Thin Solid Films, 391 (2001) 28–35.

[39] M. Shkir, I.M. Ashraf, A. Khan, M.T. Khan, A.M. El-Toni, S. AlFaify, A facile spray pyrolysis fabrication of Sm:CdS thin films for high-performance photodetector applications, Sensors and Actuators A: Physical, 306(2020)111952.

[40] A. Khan, M. Shkir, M.A. Manthrammel, V. Ganesh, I.S. Yahia, M. Ahmed, A.M. El-Toni, A. Aldalbahi, H. Ghaithan, S. AlFaify, Effect of Gd doping on structural, optical properties, photoluminescence, and electrical characteristics of CdS nanoparticles for optoelectronics. Ceram. Int., 45(2019)10133–10141.

[41] Mohd. Shkir, Ziaul Raza Khan, Kamlesh V. Chandekar, T. Alshahrani, Ashwani Kumar, S. AlFaify, A facile microwave synthesis of Cr doped CdS QDs and investigation of their physical properties for optoelectronic applications. Applied Nanoscience, 10 (2020) 3973–3985

[42] M. El-Hagary, Essam R. Shaaban, Said Moustafa, Gad Gad, Variations of energy band gap and magnetic properties upon quantum confinement effects on the Cr doped ZnO nanoparticles, Materials Research Express, 6 (2018)015030.

[43] Guomei Tang, Hua Liu and Wei Zhang, The Variation of Optical Band Gap for ZnO:In Films Prepared by Sol-Gel Technique, Advances in Materials and Science and Engineering, 2013(2013)348601.

[44] Vanita Devi, B.C.Joshi, Manish Kumar,R.J.Choudhary, Structural and optical properties of Cd and Mg doped zinc oxide thin films deposited by pulsed laser deposition, Journal of Physics: Conference Series, 534(2014)012047.

[45] L. Shen, C.Shen, J.Yang, F.Xu, Z.Q.Ma, Mechanism of blue shift of optical band gap in aluminium -doped ZnO thin films with blend bond, Materials Science Forum, 685(2011)98-104.

[46] Abderrahim El Mragui, Yuliya Logvina , Luis Pinto da Silva, Omar Zegaoui and Joaquim C.G.Esteves da Silva, Synthesis of Fe- and Co-Doped TiO_2 with Improved Photocatalytic Activity Under Visible Irradiation Toward Carbamazepine Degradation, Materials, 12(2019)3874.

[47] E. Burstein, "Anomalous optical absorption limit in InSb," Physical Review, 93 (1954)632-633.

[48] T. S. Moss, The interpretation of the properties of indium antimonide, Proceedings of the Physical Society B, 67 (1954)775-782.

[49] N.N. Greenwood and A. Eanshaw, Chemistry of the Elementa, 2nd Edn., Pergamon press, Oxford, England (1997).

[50] F.A. Cotton, G. Wilkinson, C.A. Murillo and M. Buchmann, Advanced Inorganic Chemistry, 6th Edn., New York, USA (1999).

Egyptian Journal of Solids (Egypt J. Sol.)